Journal of the Brazilian Society of Mechanical Sciences and Engineering (2018) 40:387
https://doi.org/10.1007/s40430-018-1297-z

TECHNICAL PAPER

On three-dimensional MHD Oldroyd-B fluid flow with nonlinear thermal radiation and homogeneous–heterogeneous reaction

Dianchen Lu[1] · M. Ramzan[2,4] · M. Bilal[3] · Jae Dong Chung[4] · Umer Farooq[1,5] · Saad Tahir[6]

Received: 4 March 2018 / Accepted: 8 July 2018 / Published online: 21 July 2018

Abstract

This exploration studies a new mathematical model that highlights the impact of homogeneous–heterogeneous reactions on the flow of three-dimensional Oldroyd-B fluid past a bidirectional stretched surface. Here, homogeneous reaction is described by cubic autocatalysis and heterogeneous reaction is indicated by first-order process. Additional impacts of nonlinear thermal radiation and variable thermal conductivity are also taken into account. Flow analysis is materialized in attendance of magnetohydrodynamic, heat generation/absorption and free convection. Convective heat boundary condition is also engaged in the present problem. Homotopy analysis method is betrothed to elucidate the nonlinear system of partial differential equations. A comparison to a previously done study is also added to substantiate existing results; hence, dependable results are being exhibited. Graphs of important parameters versus all distributions are also given to elucidate their physical aspects. It is reported that temperature profile is an increasing function of Biot number. It is further noted that impact of strength of homogeneous and heterogeneous reactions on concentration profile are conflicting.

Keywords Homogenous–heterogeneous reactions · Variable thermal conductivity · Nonlinear thermal radiation · Heat generation/absorption · MHD

List of symbols

A, B	Chemical species
a_0, a, b	Dimensional constant
c, d	Stretching ratio constants
B_0	Magnetic field
C_p	Specific heat
D_A	Diffusion coefficient
D_B	Diffusion coefficient
f', g'	Dimensionless velocities
Gr_x	Local Grashof number
h_f	Heat transfer coefficient
k_h	Thermal conductivity
k_c, k_s	Rate constants
k_w	Free thermal conductivity
k_∞	Free stream conductivity
M	Magnetic parameter
Nu_x	Nusselt number
Pr	Prandtl number
Q	Heat generation parameter
Q^*	Heat generation/absorption coeff
q_r	Radiative heat flux
q_w	Surface heat flux
Rd	Thermal radiation parameter
Re_x	Reynolds number
S	Deborah number
Sc	Schmidt number
T	Temperature of fluid
T_w	Wall temperature
T_∞	Ambient temperature

Technical Editor: Cezar Negrao.

✉ M. Ramzan
mramzan@bahria.edu.pk

[1] Department of Mathematics, Faculty of Science, Jiangsu University, Zhenjiang, Jiangsu, China

[2] Department of Computer Science, Bahria University, Islamabad Campus, Islamabad 44000, Pakistan

[3] Department of Mathematics, Faculty of Computing, Capital University of Science and Technology, Islamabad, Pakistan

[4] Department of Mechanical Engineering, Sejong University, Seoul 143-747, Korea

[5] Department of Mathematics, COMSATS Institute of Information Technology, Park Road Tarlai Kalan, Islamabad 45550, Pakistan

[6] School of Mechanical and Manufacturing Engineering (SMME), National University of Sciences and Technology (NUST), H-12 Campus, Islamabad, Pakistan

(u, v, w)	Velocity components
$U_w(x)$	Stretching velocity along x-axis
$V_w(y)$	Stretching velocity along y-axis
(x, y, z)	Coordinate axis
α	Variable thermal diffusivity
β	Solutal expansion coefficient
β_1	Relaxation Deborah number
β_2	Retardation Deborah number
γ_1	Strength of homogeneous reaction
γ_2	Strength of heterogeneous reaction
δ	Biot number
σ	Electrical conductivity
ρ	Density of fluid
λ	Stretching rate ratio
λ_1	Fluid relaxation time
λ_2	Fluid retardation time
λ_3	Thermal relaxation time
ν	Kinematic viscosity
θ	Dimensionless temperature
θ_w	Temperature ratio parameter
η	Similarity variable
ϕ	Dimensionless concentration
ζ	Diffusion coefficient ratio
ϵ	Thermal conductivity parameter

1 Introduction

Non-Newtonian fluids have diverse engineering and industrial applications like paper production, biomechanics, oil drilling and plastic production. Many examples of non-Newtonian fluid may be quoted like applesauce, suspension and colloidal solutions, tomato ketchup, sugar solution, exotic lubricants, condensed milk, soaps, cosmetic products and clay coatings. No single constitutive relation can exhibit varied physical structures of these fluids. In general, non-Newtonian fluids [1–10] are categorized into three leading groups: the integral type; the differential type; and the rate type. A good number of attempts in case of differential type fluids can be quoted because mathematical modeling of such fluids is much simpler in comparison with rate type fluids. Differential type fluids describe shear stress in the form of velocity components. However, very few attempts may be found in the recent literature's survey discussing rate type fluids. Maxwell fluid is a rate type fluid that only provides information about relaxation time but no information regarding retardation time. Nevertheless, Oldroyd-B fluid [11] has the ability to provide information about both relaxation and retardation times. This fluid model shows viscoelastic physiognomies of dilute polymeric solutions with normal flow conditions. Some latest attempts discussing Oldroyd-B fluid flows include a study by Hayat et al. [12]. They examined the impact of homogeneous and heterogeneous (h–h) reactions on two-dimensional MHD Oldroyd-B fluid in the presence of Cattaneo–Christov heat flux model. Then, Shehzad et al. [13] analyzed analytical solution of 3D Oldroyd-B fluid flow in attendance of Cattaneo–Christov heat flux. This was followed by an exploration by Mahanthesh et al. [14] who computed numerical solution of 3D Oldroyd-B fluid flow with heat generation/absorption and nonlinear thermal radiation past a surface which is stretched in a nonlinear way. Afterward, Sandeep and Reddy [15] analyzed numerically MHD flow of Oldroyd-B fluid across a horizontal surface in attendance of thermal and solutal stratification and cross-diffusion. Then, Mustafa [16] obtained analytical solution of mixed convective Oldroyd-B fluid with non-Fourier heat flux approach. Recently, Hayat et al. [17] discussed analytical solution of time-dependent 2D Oldroyd- B fluid flow past a non-porous stretched surface with impacts of nonlinear thermal radiation and Joule heating. Effects of heat generation/absorption with viscous dissipation with zero mass flux at the surface and convective heat conditions are also considered.

There are several chemical reacting systems which involve a number of h–h reactions occurring simultaneously. Fewer reactions proceed very sluggishly or even not at all unless a catalyst is present there. Since the h–h reactions interact in the system, therefore, the rate of product formation and reactant species' consumption varies with time. These reactions may include crops damage via freezing, hydrometallurgical industry, fog formation and dispersion, chemical processing equipment design and chemical processing equipment design. Recently, great interest in this thought-provoking idea is seen by researchers and scientists. Among these, Ramzan et al. [18] studied numerical solution of 2D magnetohydrodynamic flow of Williamson fluid near stagnation point in attendance of h–h reactions and Cattaneo–Christov heat flux with convective conditions at the boundary. Then, Hayat et al. [19] examined the series solution of the flow of second-grade fluid past a stretched cylinder in the presence of h–h reactions, Joule heating and viscous dissipation. Later, Yasmeen et al. [20] elaborated the flow of ferrofluid with effects of h–h reactions and magnetic dipole over a linearly stretching surface. This was followed by a study by Maria et al. [21] who discussed series solution of Jeffrey fluid with h–h reactions in attendance of convective boundary condition and applied magnetic field and many therein [22–26].

It is noted that most of the literature available on the subject deals with influence of homogeneous–heterogeneous reactions in varied scenarios in two-dimensional flows. Fewer explorations are also available discussing impact of h–h reactions in 3D. But no study so far has been carried out taking into account simultaneous effects of both homogeneous heterogeneous reactions and nonlinear

thermal radiation in the three-dimensional Oldroyd-B fluid flow in the presence of heat generation/absorption. Additional effects of variable thermal conductivity and magnetohydrodynamic with convective boundary condition are also taken into consideration. This study may be the first in its own capacity. Homotopy analysis method (HAM) [27–31] is employed to solve highly nonlinear system of equations. The behavior of different sundry parameters on velocity, temperature and concentration fields is highlighted with graphical illustrations. Comparison to a previous study in limiting case is also made to corroborate our results.

2 Mathematical formulation

We assume 3D flow of MHD Oldroyd-B fluid with simultaneous effects of h–h reactions and nonlinear thermal radiative heat flux occupying the region $z \geq 0$, past a surface stretched along x and $y$directions with velocities $u = ax$ and $v = by$, respectively. It is further assumed that temperature far away from the surface T_∞ is much smaller as compared to the temperature at the surface T_w. Along z-axis, fluid is taken electrically conducting in attendance of constant magnetic field Bo as shown in Fig. 1. Because of our supposition of small Reynolds number, induced magnetic field is overlooked. A nonlinear thermal diffusivity and the effect of heat generation absorption are considered during the formulation of energy equation. Modified Fourier's law known as Cattaneo–Christov heat flux model is used to see the behavior of thermal relaxation time during non-Newtonian fluid flow. It is further assumed that the temperature of the bidirectional stretching sheet is maintained constant by considering the convective boundary condition. An investigation of two chemical species A and B with h–h reactions is performed. For cubic autocatalysis, the homogeneous reaction is given by [8]

$$A + 2B \rightarrow 3B, \text{ rate } = k_c ab^2. \tag{1}$$

However, on the catalyst surface there is only heterogeneous reaction represented by:

$$A \rightarrow B, \text{ rate } = k_s a, \tag{2}$$

where k_c, k_s and a, b are rate constants and concentrations of the chemical species A and B, respectively. The constitutive equations of Oldroyd-B fluid (incompressible) model are appended by

$$\text{div}\mathbf{V} = 0, \tag{3}$$

$$\rho \frac{\mathrm{d}\mathbf{V}}{\mathrm{d}t} = \text{div}\mathbf{T}. \tag{4}$$

Here, extra stress tensor $\mathbf{S}$ and the Cauchy stress tensor $\mathbf{T}$ are defined as

$$\mathbf{T} = -p\mathbf{I} + \mathbf{S}, \tag{5}$$

$$\mathbf{S} = \lambda_1 \frac{D\mathbf{S}}{Dt} = \mu\left(A_1 + \lambda_2 \frac{DA_1}{Dt}\right), \tag{6}$$

with D / Dt is the covariant differentiation and fluid relaxation and retardation time is represented by λ_1 and λ_2, respectively. The first Rivlin–Ericksen tensor A_1 is defined as

$$A_1 = \text{grad}\mathbf{V} + (\text{grad}\mathbf{V})', \tag{7}$$

where $'$ specifies the matrix transpose and the velocity field $\mathbf{V}$ is represented by

$$\mathbf{V} = [u(x, y, z), v(x, y, z), w(x, y, z)], \tag{8}$$

The derivative D / Dt is [32] given by

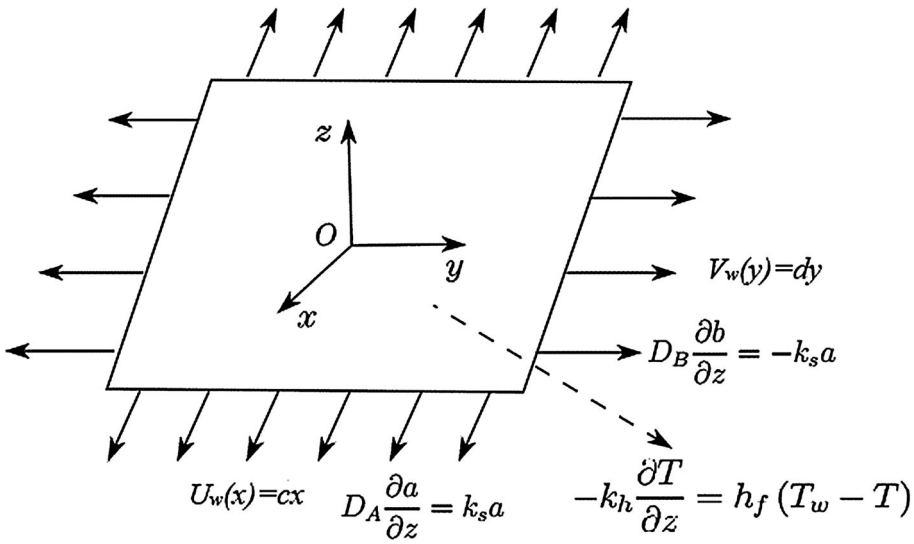

Fig. 1 Geometry of the problem

$$\frac{Da_i}{Dt} = \frac{\partial a_i}{\partial t} + u_r a_{i,r} - u_{i,r} a_r. \tag{9}$$

the energy and the species equations in the vector form are defined as

$$\rho C_p (V.\nabla T) = \nabla.q - \nabla q_r + Q^*(T - T_\infty) \tag{10}$$

with q is heat flux and is defined by the Cattaneo–Christov model as

$$q + \lambda_3 \left[\frac{\partial q}{\partial t} + V.\nabla q - q.\nabla V + (\nabla.V)q \right] = \nabla(kT) \tag{11}$$

The species concentration equations in the vector form are defined as

$$V.\nabla a = D_A^2 \nabla a - k_c a b^2 \tag{12}$$

$$V.\nabla b = D_B^2 \nabla b + k_c a b^2 \tag{13}$$

Following the instructions given in [32] and then adopting the boundary layer postulations [33], we have [14, 34]:

$$\frac{\partial u}{\partial x} + \frac{\partial \upsilon}{\partial y} + \frac{\partial w}{\partial z} = 0, \tag{14}$$

$$\begin{aligned} &u\frac{\partial u}{\partial x} + \upsilon\frac{\partial u}{\partial y} + w\frac{\partial u}{\partial z} \\ &+ \lambda_1 \left(\begin{array}{c} u^2\frac{\partial^2 u}{\partial x^2} + \upsilon^2\frac{\partial^2 u}{\partial y^2} + w^2\frac{\partial^2 u}{\partial z^2} + \\ 2u\upsilon\frac{\partial^2 u}{\partial x \partial y} + 2\upsilon w\frac{\partial^2 u}{\partial y \partial z} + 2uw\frac{\partial^2 u}{\partial x \partial z} \end{array} \right) \\ &= \nu \left(\frac{\partial^2 u}{\partial z^2} + \lambda_2 \left(\begin{array}{c} u\frac{\partial^3 u}{\partial x \partial z^2} + \upsilon\frac{\partial^3 u}{\partial y \partial z^2} + w\frac{\partial^3 u}{\partial z^3} - \\ \frac{\partial u}{\partial x}\frac{\partial^2 u}{\partial z^2} - \frac{\partial u}{\partial y}\frac{\partial^2 \upsilon}{\partial z^2} - \frac{\partial u}{\partial z}\frac{\partial^2 w}{\partial z^2} \end{array} \right) \right) \\ &- \frac{\sigma B_o^2}{\rho}\left(u + \lambda_1 w\frac{\partial u}{\partial z} \right) + g\beta(T - T_\infty), \end{aligned} \tag{15}$$

$$\begin{aligned} &u\frac{\partial \upsilon}{\partial x} + v\frac{\partial \upsilon}{\partial y} + w\frac{\partial \upsilon}{\partial z} \\ &+ \lambda_1 \left(\begin{array}{c} u^2\frac{\partial^2 \upsilon}{\partial x^2} + v^2\frac{\partial^2 \upsilon}{\partial y^2} + w^2\frac{\partial^2 \upsilon}{\partial z^2} + \\ 2uv\frac{\partial^2 \upsilon}{\partial x \partial y} + 2vw\frac{\partial^2 \upsilon}{\partial y \partial z} + 2uw\frac{\partial^2 \upsilon}{\partial x \partial z} \end{array} \right) \\ &= \nu \left(\frac{\partial^2 \upsilon}{\partial z^2} + \lambda_2 \left(\begin{array}{c} u\frac{\partial^3 \upsilon}{\partial x \partial z^2} + v\frac{\partial^3 \upsilon}{\partial y \partial z^2} + w\frac{\partial^3 \upsilon}{\partial z^3} - \\ \frac{\partial \upsilon}{\partial x}\frac{\partial^2 \upsilon}{\partial z^2} - \frac{\partial \upsilon}{\partial y}\frac{\partial^2 \upsilon}{\partial z^2} - \frac{\partial \upsilon}{\partial z}\frac{\partial^2 w}{\partial z^2} \end{array} \right) \right) \\ &- \frac{\sigma B_o^2}{\rho}\left(v + \lambda_1 w\frac{\partial \upsilon}{\partial z} \right), \end{aligned} \tag{16}$$

$$\begin{aligned} &u\frac{\partial T}{\partial x} + \upsilon\frac{\partial T}{\partial y} + +w\frac{\partial T}{\partial z} = \frac{1}{\rho C_P}\frac{\partial}{\partial z}\left(\alpha\frac{\partial T}{\partial z} \right) \\ &- \lambda_3 \left(\begin{array}{c} u^2\frac{\partial^2 T}{\partial x^2} + \upsilon^2\frac{\partial^2 T}{\partial y^2} + w^2\frac{\partial^2 T}{\partial z^2} + 2u\upsilon\frac{\partial^2 T}{\partial x \partial y} \\ +2\upsilon w\frac{\partial^2 T}{\partial y \partial z} + 2uw\frac{\partial^2 T}{\partial x \partial z} + \left(u\frac{\partial u}{\partial x} + \upsilon\frac{\partial u}{\partial y} + w\frac{\partial u}{\partial z} \right)\frac{\partial T}{\partial x} + \\ \left(u\frac{\partial \upsilon}{\partial x} + \upsilon\frac{\partial \upsilon}{\partial y} + w\frac{\partial \upsilon}{\partial z} \right)\frac{\partial T}{\partial y} + \left(u\frac{\partial w}{\partial x} + \upsilon\frac{\partial w}{\partial y} + w\frac{\partial w}{\partial z} \right)\frac{\partial T}{\partial z} \end{array} \right) \\ &- \frac{1}{\rho C_p}\frac{\partial q_r}{\partial z} + \frac{Q^*}{\rho C_P}(T - T_\infty), \end{aligned} \tag{17}$$

$$u\frac{\partial a}{\partial x} + v\frac{\partial a}{\partial y} + w\frac{\partial a}{\partial z} = D_A\frac{\partial^2 a}{\partial z^2} - k_c a b^2, \tag{18}$$

$$u\frac{\partial b}{\partial x} + v\frac{\partial b}{\partial y} + w\frac{\partial b}{\partial w} = D_B\frac{\partial^2 b}{\partial z^2} + k_c a b^2, \tag{19}$$

with u, v and w are the velocities along x-, y- and $z-$ axes, respectively. Here, $v, \sigma, B_0, T, C_p, \rho, D_A, D_B, \lambda_3, \alpha$ and λ_1 denote kinematic viscosity, electrical conductivity, uniform magnetic field, temperature, specific heat, fluid density, diffusion coefficients, thermal relaxation time, variable thermal conductivity and retardation time, respectively. Equations (10–15) are supported by the boundary conditions given below

$$\left. \begin{array}{l} u = cx,\ \upsilon = dy, w = 0,\ -k_h\frac{\partial T}{\partial z} = h_f(T_w - T), \\ D_A\frac{\partial a}{\partial z} = k_s a,\ D_B\frac{\partial b}{\partial z} = -k_s a, \text{at } z = 0, \\ u \to 0, \upsilon \to 0,\ a \to a_o,\ b \to 0,\ T \to T_\infty \text{ as } z \to \infty, \end{array} \right\} \tag{20}$$

where h_f and k_h are heat transfer coefficient and thermal conductivity with a, b and a_0 are positive-dimensional constants. Using the following transformations [35]

$$\left. \begin{array}{l} u = U_w(x) = cxf'(\eta), \upsilon = V_w(y) = cyg'(\eta), w = \\ -\sqrt{c\nu}(f(\eta) + g(\eta)), \\ \theta(\eta) = \frac{T - T_\infty}{T_w - T_\infty}, \eta = \sqrt{\frac{c}{\nu}}z, b = a_0 h(\eta), a = a_0\phi(\eta). \end{array} \right\} \tag{21}$$

The variable thermal conductivity [35] is given by $\epsilon = \frac{k_w - k_\infty}{k_\infty}$ with k_∞ and k_w are the fluid-free stream conductivity and the thermal conductivity at wall, respectively, also in Eq. $T = T_\infty((\theta_w - 1)\theta(\eta) + 1)$, with $\theta_w = \frac{T_w}{T_\infty}$. Using above transformations, requirement of Eq. (10) is fulfilled spontaneously, nevertheless, Eqs. (11–16) take the form

$$f''' + \left(M^2\beta_1 + 1\right)(f+g)f'' - f'^2 - M^2 f' + \beta_1\left(2(f+g)f'f'' - (f+g)^2 f'''\right) + \beta_2((f''+g'')f'' - (f+g)f'''') + Gr_x\theta = 0, \tag{22}$$

$$g''' + \left(M^2\beta_1 + 1\right)(f+g)g'' - g'^2 - M^2 g' + \beta_1\left(2(f+g)g'g'' - (f+g)^2 g'''\right) + \beta_2((f''+g'')g'' - (f+g)g'''') = 0, \tag{23}$$

$$(1+\epsilon\theta)\theta'' + \epsilon\theta'^2 + Pr(f+g)\theta' - PrS\left((f+g)^2\theta'' + (f+g)(f'+g')\theta'\right) + \Pr Q\theta + \frac{4}{3}Rd((\theta_w-1)\theta+1)^3\theta'' + 4Rd(\theta_w-1)((\theta_w-1)\theta+1)^2\theta'^2 = 0, \tag{24}$$

$$\phi'' + Sc(f+g)\phi' - Sc\gamma_1\phi h^2 = 0, \tag{25}$$

$$\zeta h'' + Sc(f+g)h' + Sc\gamma_1\phi h^2 = 0, \tag{26}$$

$$\left.\begin{aligned} &f(0)=0,\ f'(0)=1, g(0)=0, g'(0)=\lambda, \phi'(0)=\gamma_2\phi(0),\\ &\theta'(0) = -\delta(1-\theta(0)), \zeta h'(0) = -\gamma_2\phi(0),\\ &f'(\infty)\to 0,\ f''(\infty)\to 0, g'(\infty)\to 0, g''(\infty)\to 0,\\ &\phi(\infty)\to 1,\ h(\infty)\to 0, \theta(\infty)\to 0, \end{aligned}\right\} \tag{27}$$

where $Pr, Gr_x, M, \theta_w, \epsilon, \delta, Q, \beta_1$ and $\beta_2, Sc, Rd, \lambda, \gamma_1$ and γ_2, ζ and S are the Prandtl number, local Grashof number, magnetic field strength, temperature ratio parameter, thermal conductivity parameter, Biot number, heat generation/absorption parameter, Deborah numbers in terms of relaxation and retardation time, Schmidt number, thermal radiation parameter, ratio of stretching rate, measure of strength of homogenous and heterogeneous reactions, ratio of diffusion coefficient and Deborah number w.r.t relaxation time of heat flux. The values of these parameters are given below:

$$\left.\begin{aligned} &Pr = \frac{\mu C_p}{k},\ M^2 = \frac{\sigma B_o^2}{\rho c}, \delta = \frac{h_f}{k}\sqrt{\frac{\nu}{c}}, \beta_1 = \lambda_1 a,\ \beta_2 = \lambda_2 a, \theta_w = \frac{T_w}{T_\infty},\\ &Rd = \frac{4\sigma^* T_\infty^3}{kk^*}, Re_x = \frac{u_w x}{\nu}, Q = \frac{Q^*}{c\rho C_P}, Gr_x = \frac{g\beta(T_w - T_\infty)}{c^2 x},\\ &Sc = \frac{\nu}{D_A},\ \lambda = \frac{d}{c}, \gamma_1 = \frac{k_c a_0^2}{c}, \gamma_2 = \frac{k}{D_A}\sqrt{\frac{\nu}{c}},\ \zeta = \frac{D_B}{D_A}, S = \lambda_3 a. \end{aligned}\right\} \tag{28}$$

The result that D_A and D_B are same, *i.e.*, $\zeta = 1$ is because of our supposition that diffusion coefficients related to chemical species A and B are having the same size. That is why we have

$$\phi(\eta) + h(\eta) = 1. \tag{29}$$

Now, Eqs. (21) and (22) yield

$$\phi'' + Sc(f+g)\phi' - Sc\gamma_1\phi(1-\phi)^2 = 0, \tag{30}$$

with boundary conditions

$$\phi'(0) = \gamma_2\phi(0),\ \phi(\infty) = 1. \tag{31}$$

The local Nusselt number in dimensional form is given by

$$Nu_x = \frac{xq_w}{k(T_w - T_\infty)}, \tag{32}$$

where

$$q_w = -k\left(\frac{\partial T}{\partial z}\right) + q_r\Big|_{z=0}. \tag{33}$$

Dimensionless form of Nusselt number is

$$Nu_x Re_x^{-1/2} = -\left(1 + \frac{4}{3}Rd((\theta_w-1)\theta(0)+1)^3\right)\theta'(0). \tag{34}$$

3 Homotopic solutions

There are many numerical and analytical techniques which can be used to solve the system of Eqs. (22–26). Among these, the most commons are finite difference method [36] shooting method [37, 38] Fehlberg–Runge–Kutta integration [39] Successive linearization method [40]. The choice of Homotopy analysis method (HAM) is because of its edge on the other contemporary techniques. The HAM is a powerful analytical method, suggested by Liao [41] in 1992, has following advantages in comparison with the other techniques;

- It is independent of the choice of small or large parameter.
- The convergence in case of HAM is guaranteed.
- An ample choice to select the initial guess estimates and the respective operators.

The preliminary guess estimates $(f_0, g_0, \theta_0, \phi_0)$ and linear operators $\left(\mathcal{L}_f, \mathcal{L}_g, \mathcal{L}_\theta, \mathcal{L}_\phi\right)$ required for Homotopy analysis method are defined as:

$$\left.\begin{aligned} &f_0(\eta) = (1-\exp(-\eta)), g_0(\eta) = \lambda(1-\exp(-\eta)),\\ &\theta_0(\eta) = \frac{\delta\exp(-\eta)}{1+\delta}, \phi_0(\eta) = 1 - \frac{1}{2}\exp(-\gamma_2\eta), \end{aligned}\right\} \tag{35}$$

and

$$\mathcal{L}_f(\eta) = \frac{d^3 f}{d\eta^3} - \frac{df}{d\eta},\ \mathcal{L}_g(\eta) = \frac{d^3 g}{d\eta^3} - \frac{dg}{d\eta},\ \mathcal{L}_\theta(\eta) = \frac{d^2\theta}{d\eta^2} - \theta, \mathcal{L}_\phi(\eta) = \frac{d^2\phi}{d\eta^2} - \phi. \tag{36}$$

with the following properties

$$\left.\begin{aligned} &\mathcal{L}_f[C_1 + C_2\exp(\eta) + C_3\exp(-\eta)] = 0,\\ &\mathcal{L}_g[C_4 + C_5\exp(\eta) + C_6\exp(-\eta)] = 0,\\ &\mathcal{L}_\phi[C_7\exp(\eta) + C_8\exp(-\eta)] = 0,\\ &\mathcal{L}_\theta[C_9\exp(\eta) + C_{10}\exp(-\eta)] = 0, \end{aligned}\right\} \tag{37}$$

where C_i $(i = 1 - 10)$, the arbitrary constants. The values of these constants using given boundary conditions are

$$\left.\begin{aligned} &C_2 = C_5 = C_7 = C_9 = 0, \qquad C_3 = \left.\frac{\partial f_m^\star(\eta)}{\partial\eta}\right|_{\eta=0},\\ &C_1 = -C_3 - f_m^\star(0) \qquad C_6 = \left.\frac{\partial g_m^\star(\eta)}{\partial\eta}\right|_{\eta=0},\\ &C_4 = -C_6 - g_m^\star(0) \qquad C_8 = \frac{1}{1+\delta}\left(\left.\frac{\partial\theta_m^*(\eta)}{\partial\eta}\right|_{\eta=0} - \delta\theta_m^*(0)\right),\\ &C_{10} = \frac{1}{1+\gamma_2}\left(\left.\frac{\partial\phi_m^*(\eta)}{\partial\eta}\right|_{\eta=0} - \gamma_2\phi_m^*(0)\right). \end{aligned}\right\} \tag{38}$$

3.1 Convergence analysis

To determine the region of convergence for series solutions, the importance of auxiliary parameters $(\hbar_f, \hbar_g, \hbar_\theta, \hbar_\phi)$ cannot be denied. In Fig. 2, illustration for $\hbar-$curves is presented to identify the same region. Tolerable ranges of parameters $\hbar_f, \hbar_g$, $\hbar_\theta$ and $\hbar_\phi$ are $-1.7 \le \hbar_f \le -0.5$, $-1.6 \le \hbar_g \le -0.4$, $-1.6 \le \hbar_\theta \le -0.4$ and $-2.0 \le \hbar_\phi \le -0.4$, respectively. The values of these parameters are in complete alignment to those numerical values found in Table 1.

Table 1 Convergence table for varied values of approximations when $\beta_1 = 0.2$, $\beta_2 = 0.2$, $M = 0.4$, $\epsilon = 0.3$, $\lambda = 0.3$, $\delta = 0.3$, Pr = 2.0, $Rd = 0.3$, $Q = 0.2$, $\Psi = 0.1$, $\theta_w = 1.3$, $S = 0.2$, $\gamma_1 = 0.4$, $\gamma_2 = 0.6$, Sc = 0.7

Order of approximations	$-f''(0)$	$-g''(0)$	$-\theta'(0)$	$\phi'(0)$
1	1.02224	0.25176	0.21056	0.28022
5	1.04802	0.25126	0.19517	0.26174
10	1.05302	0.25302	0.19537	0.25745
15	1.05523	0.25377	0.19769	0.25618
20	1.05661	0.25413	0.19973	0.25570
25	1.05755	0.25432	0.20122	0.25551
30	1.05783	0.25438	0.20168	0.25548
35	1.05792	0.25441	0.20173	0.25543
40	1.05792	0.25441	0.20174	0.25543

Table 2 Local Nusselt number $-\theta'(0)$ in the absence of homogeneous heterogeneous reactions, variable thermal conductivity, magnetohydrodynamic, heat generation and nonlinear thermal radiation when compared with Hayat et al. [34] for $\beta = 0.5$

β_1	β_2	Pr	δ	[34]	Present
0.0	0.4	1.0	0.8	0.39658	0.39658
0.5	0.4	1.0	0.8	0.38228	0.38228
1.0	0.4	1.0	0.8	0.36997	0.36997
0.4	0.0	1.0	0.8	0.36761	0.36761
0.4	0.5	1.0	0.8	0.38793	0.38793
0.4	1.0	1.0	0.8	0.39552	0.39552
0.4	0.4	0.5	0.8	0.29221	0.29221
0.4	0.4	0.8	0.8	0.35506	0.35506
0.4	0.4	1.3	0.8	0.41932	0.41932
0.4	0.4	1.0	0.3	0.21365	0.21365
0.4	0.4	1.0	0.6	0.33187	0.33187
0.4	0.4	1.0	1.0	0.42614	0.42614

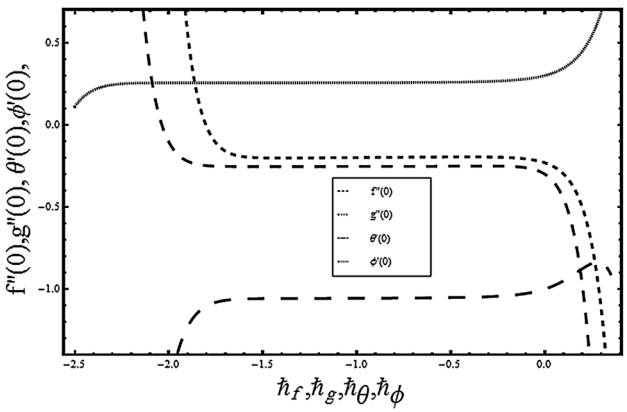

Fig. 2 $\hbar$ for the function f, g, θ, ϕ

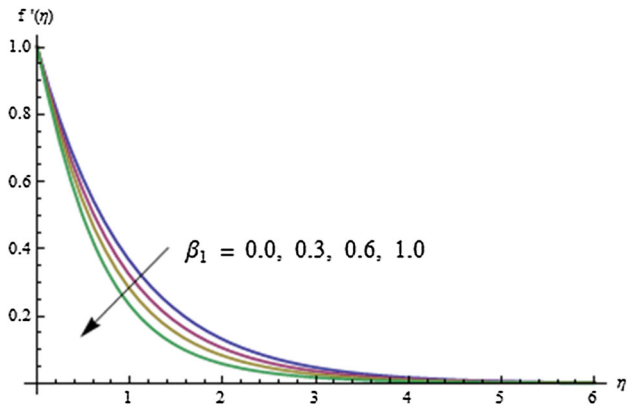

Fig. 3 Graph of β_1 versus $f'(\eta)$

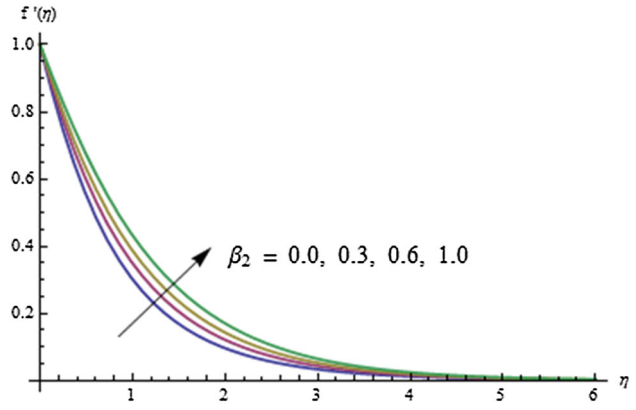

Fig. 4 Graph of β_2 versus $f'(\eta)$

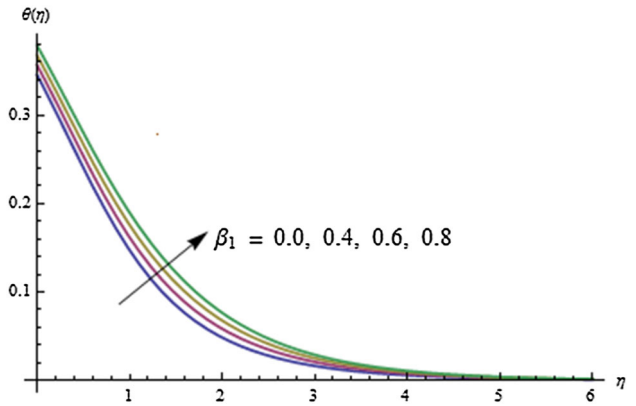

Fig. 5 Graph of β_1 versus $\theta(\eta)$

4 Results and discussion

Figures (3, 4, 5, 6, 7, 8, 9, 10, 11, 12, 13, 14, 15 and 16) depict the behavior of emerging parameters on velocity, temperature and concentration distributions. All the computation is carried out for the following ranges of physical parameters [42] $\beta_1(0.0 \le \beta_1 \le 1.0), \beta_2(0.0 \le \beta_2 \le 1.0), Pr(\le 0.0 Pr \le 6.0), \epsilon(0.0 \le \epsilon \le 3.0), \gamma_1(0.0 \le \gamma_1 \le 3.0), \gamma_2(0.1 \le \gamma_2 \le 0.9), \delta(0.2 \le \delta \le 1.0), M(0.0 \le M \le 1.5), Rd(0.2 \le Rd \le 1.0), Q(0.2 \le Q \le 0.8), Gr(0.0 \le Gr \le 3.0), \theta_w(1.0 \le \theta_w \le 2.0), S(0.1 \le S \le 3.0)$ From Fig. 3, it is witnessed that the fluid velocity along the $x-$axis, *i.e.*, $f'(\eta)$ is a decreasing function of "Deborah number for relaxation time" β_1. Since, relaxation time and Deborah number have a direct relation. That is why higher relaxation time results in larger Deborah number which resist the flow of the fluid and ultimately lowers the fluid velocity distributions. In comparison, it is observed that both β_1 and β_2 have an opposite effect on velocity distribution. β_2 namely known as "Deborah number for retardation time" have an increasing trend for the velocity profile. As by the definition of β_2, it is directly related with the retardation time

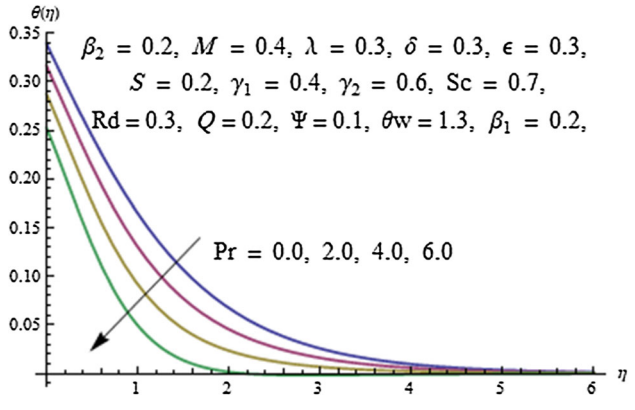

Fig. 6 Graph of Pr versus $\theta(\eta)$

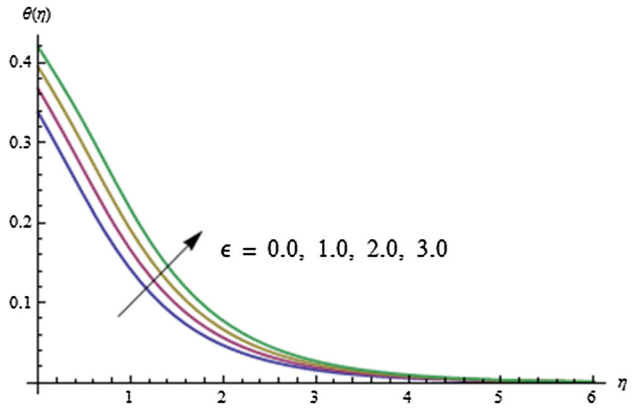

Fig. 7 Graph of ϵ versus θ

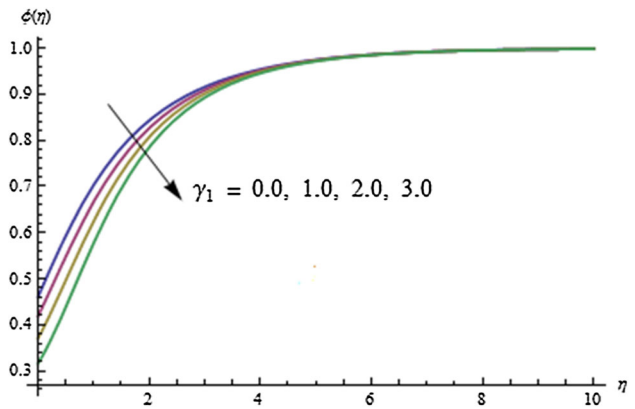

Fig. 8 Graph of γ_1 versus $\phi(\eta)$

which is defined as the delay response to an applied force or simply the "delay of the elasticity." It is observed from Fig. 4 that velocity of the fluid increases for the higher values of Deborah number β_2. Influence of Deborah number β_1 depending on relaxation time is displayed in Fig. 5. Temperature has a direct proportion to relaxation time. That is why higher values of β_1 corresponds to an

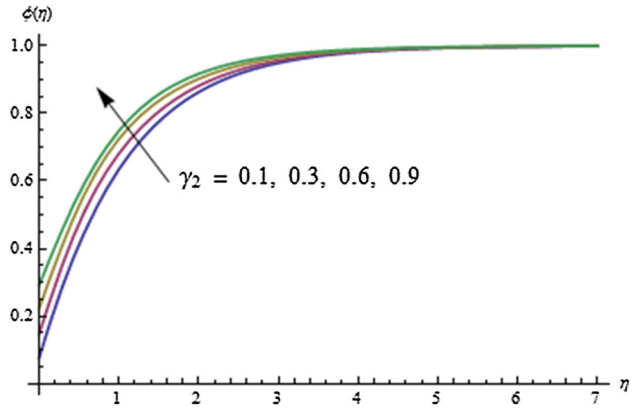

Fig. 9 Graph of γ_2 versus $\phi(\eta)$

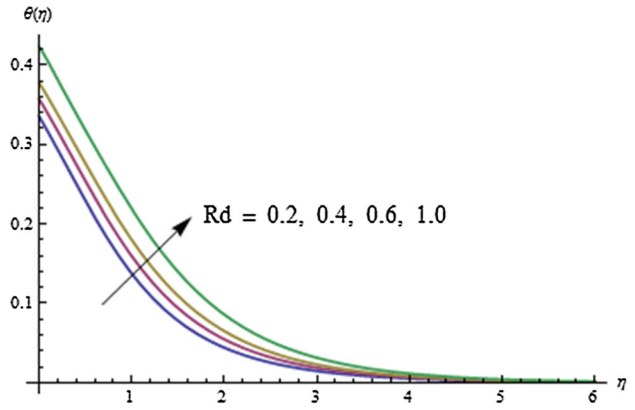

Fig. 12 Graph of Rd versus $\theta(\eta)$

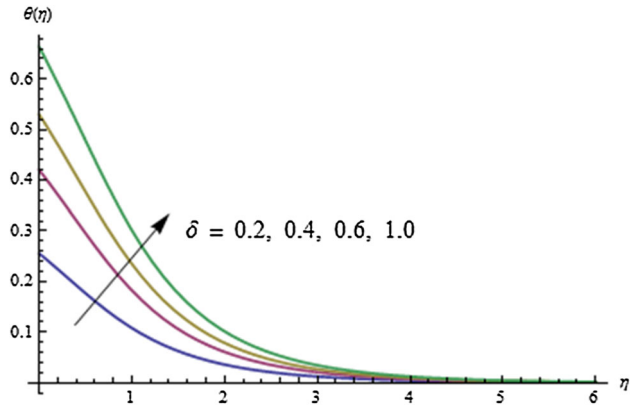

Fig. 10 Graph of δ versus $\theta(\eta)$

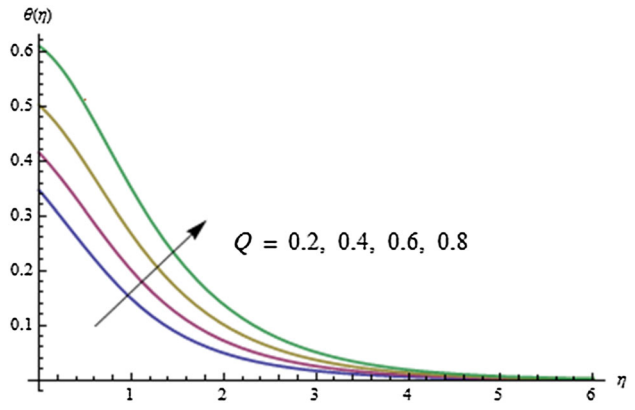

Fig. 13 Graph of Q versus $\theta(\eta)$

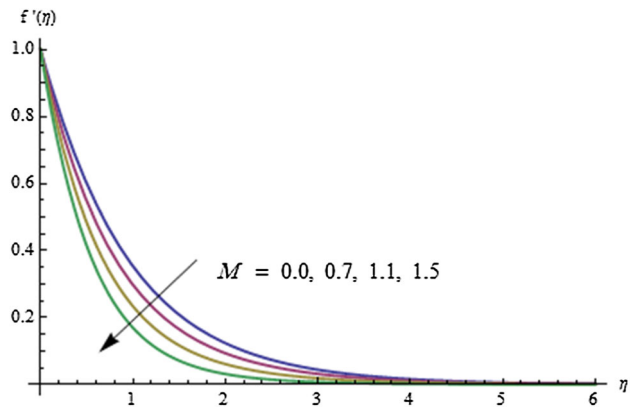

Fig. 11 Graph of M versus $f'(\eta)$

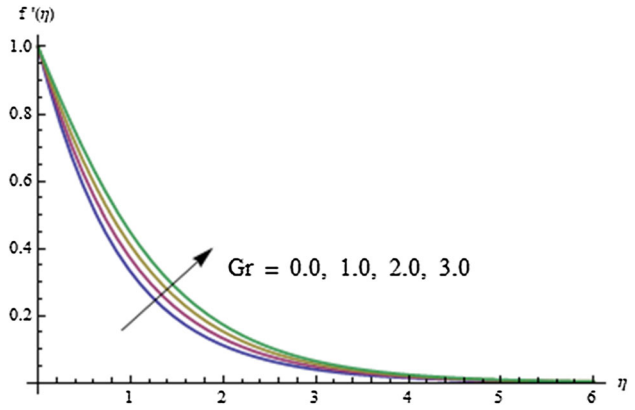

Fig. 14 Graph of Gr versus $f'(\eta)$

increase in the temperature and hence its thermal boundary layer thickness.

Figure 6 displays the impact of Prandtl number on the temperature profile. Thermal diffusivity has a reverse relation with Prandtl number. Hence, the conduction reduces for higher value of Pr which causes the reduction in temperature of the fluid. It is further observed that the large value of Pr resultantly lower the thermal boundary layer thickness. Figure 7 shows the impacts of thermal conductivity parameter ϵ on temperature field. Since, we know that liquids with higher thermal conductivity have increased temperature. The same effect may be visualized in Fig. 7. The reactants are expanded during the homogeneous reaction which triggers the reduction in concentration profile. This impact of strength of homogeneous reaction γ_1 on concentration distribution is depicted in

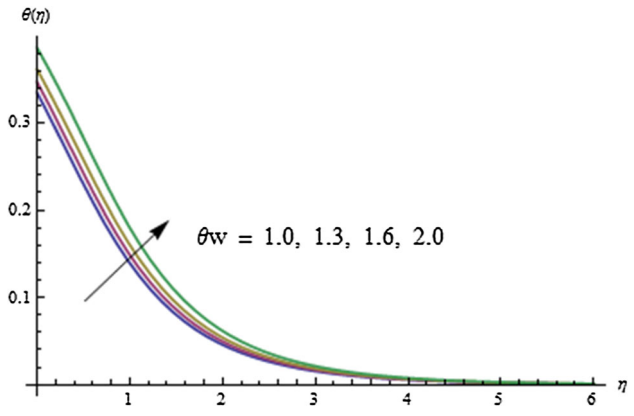

Fig. 15 Graph of θ_w versus $\theta(\eta)$

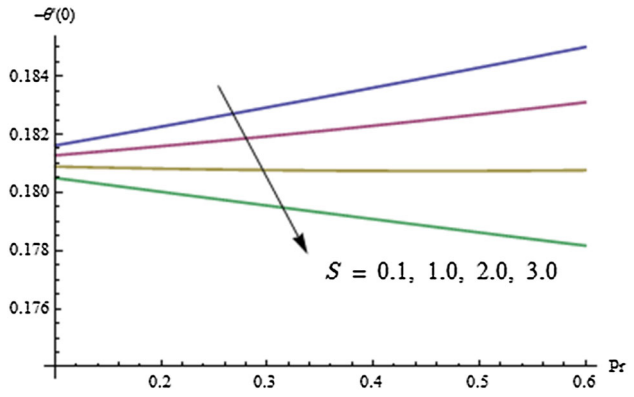

Fig. 16 Graph of Pr and S versus $Nu_x Re_x^{-\frac{1}{2}}$

Fig. 8. An opposite behavior in case of increasing values of strength of heterogeneous reaction γ_2 on concentration field is shown in Fig. 9. Here, concentration boosts because of less diffused particles. The impact of Biot number δ on the thermal boundary layer is elucidated in Fig. 10. As anticipated, the larger surface temperature is observed due to sturdier convection, instigating the thermal effect penetrating deeper into the fluid.

Figure 11 illustrates that velocity distribution function is diminishing function of magnetic field parameter M. Lorentz force generated by the applied magnetic transverse field will oppose the flow of the fluid and eventually a decrease in the velocity function is observed. Figure 12 shows the effect of radiation parameter Rd on temperature distribution. The rise in the fluid temperature is experimented because of increase in values of Rd. Actually, more heat transferred to the fluid because of high values of radiation parameter. Effect of heat generation/absorption parameter Q on the temperature field is portrayed in Fig. 13. It is perceived that temperature distribution is escalating function of Q. Fluid's temperature is on rise because of growing values of Q that eventually boosts the temperature field. Figure 14 illustrates the influence of Grashof number Gr on velocity profile. As Grashof number Gr is the quotient of buoyancy to viscous force. Higher values of Gr mean stronger buoyancy force in comparison with viscous force. This act accelerates the fluid flow and enhanced fluid's velocity is perceived.

In Fig. 15, fluid's temperature rise is observed versus increasing values of temperature ratio parameter θ_w. In fact, enhanced wall temperature is the core cause to boosts the temperature of the fluid by increasing values of θ_w. In Fig. 16, effects of both Prandtl number Pr and Deborah number with respect to relaxation time of heat flux S are presented on Nusselt number. It is witnessed that Nusselt number escalates with increasing values of Pr. However,

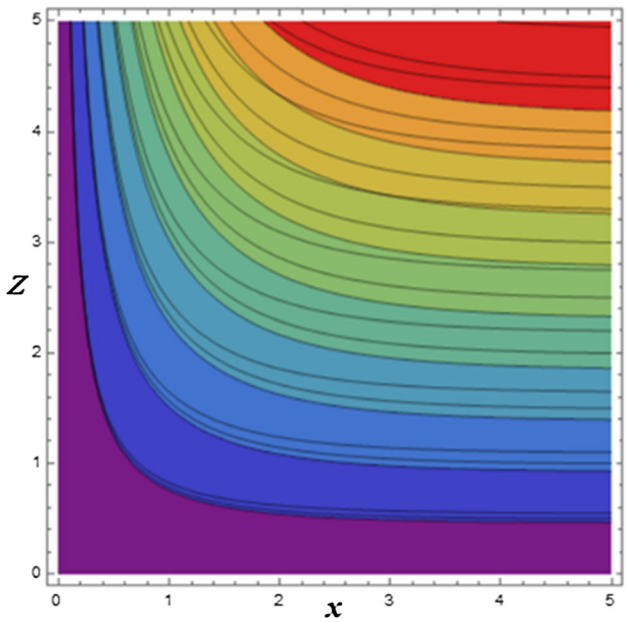

Fig. 17 Streamline graph in 2D view

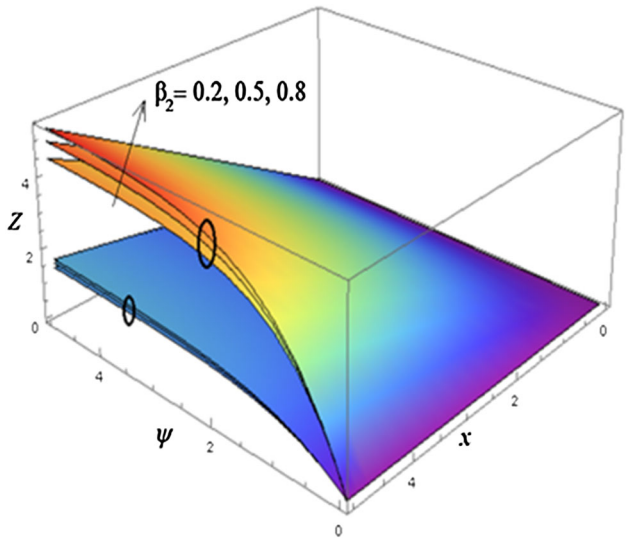

Fig. 18 3D view of streamlines for various values of β_2

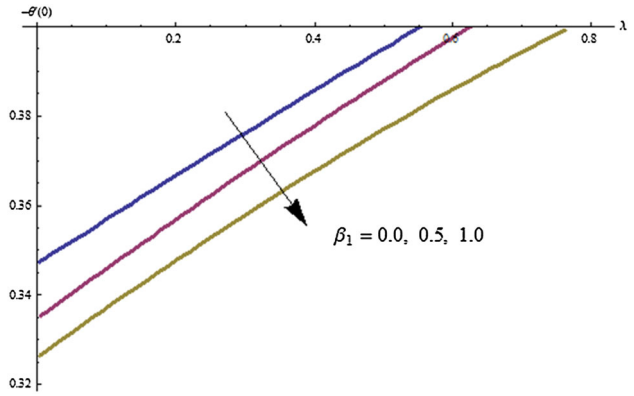

Fig. 19 Graphical comparison with [34] for varied values of β_1 and λ

an opposite behavior is observed for growing values of S. Streamlines are basically the path traced out by the fluid particles within the flow. The graphs of streamlines with 2D and 3D views for various values of β_2 are portrayed in Figs. 17 and 18, respectively. Excellent alignment in both figures is found. Figure 19 gives a comparison of $-\theta'(0)$ for various values of β_1 and λ by fixing other parameters for the first three values of Table 2 of [35]. An excellent agreement is seen in both numerical and graphical results.

5 Conclusions

In this study, simultaneous effects of h–h reactions with nonlinear radiative heat flux on the flow of 3D Oldroyd fluid past a linearly bidirectional stretched surface are pondered. Impacts of magnetohydrodynamic with heat generation/absorption in the presence of variable thermal conductivity and free convection are also considered. The important points highlighted in this investigation are appended as follows:

- Nusselt number escalates and decreases for growing values of Prandtl number and Deborah number with respect to relaxation time of heat flux , respectively.
- Effects of strength of homogeneous–heterogeneous (h–h) reactions on concentration profile are opposite, as it decreases for the strength of homogenous reaction and increases for the heterogeneous reaction.
- Thermal boundary layer escalates with increasing values of Biot number.
- Larger values of magnetic field parameter cause an enhancement in velocity field.
- Temperature filed is mounting function of thermal conductivity and thermal radiation parameters.
- For larger values of local Grashof number, velocity profile also increases.
- Temperature distribution with its associated thermal boundary layer thickness is boosted for the larger values of temperature ratio parameter.

Acknowledgements "This work was supported by the Korea Institute of Energy Technology Evaluation and Planning (KETEP) and the Ministry of Trade, Industry & Energy (MOTIE) of the Republic of Korea (No. 20172010105570)."

Compliance with ethical standard

Conflict of interest The authors declare no conflict of interest.

References

1. Koriko OK, Animasaun IL, Reddy MG, Sandeep N (2017) Scrutinization of thermal stratification, nonlinear thermal radiation and quartic autocatalytic chemical reaction effects on the flow of three-dimensional Eyring Powell alumina-water nanofluid. Multidiscip Model Mater Struct. https://doi.org/10.1108/MMMS-08-2017-0077
2. Ramzan M, Bilal M, Farooq U, Chung JD (2016) Mixed convective radiative flow of second grade nanofluid with convective boundary conditions: an optimal solution. Results Phys 6:796–804
3. Sandeep N, Reddy MG (2017) MHD Oldroyd-B fluid flow across a melting surface with cross diffusion and double stratification. Eur Phys J Plus 132:147
4. Ramzan M, Bilal M, Chung JD, Lu D, Farooq U (2017) Impact of generalized Fourier's and Fick's laws on MHD 3D second grade nanofluid flow with variable thermal conductivity and convective heat and mass conditions. Phys Fluids 29(9):093102
5. Reddy MG, Makinde OD (2016) Magnetohydrodynamic peristaltic transport of Jeffrey nanofluid in an asymmetric channel. J Mol Liq 223:1242–1248
6. Bhatti MM, Abbas T, Rashidi MM (2016) Numerical study of entropy generation with nonlinear thermal radiation on magnetohydrodynamics non-Newtonian nanofluid through a porous shrinking sheet. J Magn 21(1):468–475
7. Reddy MG (2018) Cattaneo-Christov heat flux effect on hydromagnetic radiative Oldroyd-B liquid flow across a cone/wedge in the presence of cross-diffusion. Eur Phys J Plus 133:24
8. Raju CSK, Sandeep N, Reddy MG (2015) Effect of nonlinear thermal radiation on 3D Jeffreyfluid flow in the presence of homogeneous-heterogeneous reactions. Int J Eng Res Afr 21:52–68
9. Bhatti MM, Abbas T, Rashidi MM, El-Sayed Ali M (2016) Numerical simulation of entropy generation with thermal radiation on MHD Carreau nanofluid towards a shrinking sheet. Engropy 18:200
10. Bhatti MM, Rashidi MM (2016) Effects of thermo-diffusion and thermal radiation on Williamson nanofluid over a porous shrinking/stretching sheet. J Mol Liq 221:567–573
11. Oldroyd J (1950) On the formulation of rheological equations of state. Proc R Soc A Math Phys Sci 200:523–541
12. Hayat T, Imtiaz M, Alsaedi A, Almezal S (2016) On Cattaneo-Christov heat flux in MHD flow of Oldroyd-B fluid with homogeneous-heterogeneous reactions. J Magn Magn Mater 401:296–303
13. Shehzad SA, Hayat T, Abbasi FM, Javed T, Kutbi MA (2016) Three-dimensional Oldroyd-B fluid flow with Cattaneo-Christov heat flux model. Eur Phys J Plus 131(4):112

14. Mahanthesh B, Gireesha BJ, Shehzad SA, Abbasi FM, Gorla RS (2017) Nonlinear three-dimensional stretched flow of an Oldroyd-B fluid with convective condition, thermal radiation and mixed convection. Appl Math Mech 38(7):969–980
15. Sandeep N, Reddy MG (2017) MHD Oldroyd-B fluid flow across a melting surface with cross diffusion and double stratification. Eur Phys J Plus 132:147
16. Mustafa M (2017) An analytical treatment for MHD mixed convection boundary layer flow of Oldroyd-B fluid utilizing non-Fourier heat flux model. Int J Heat Mass Transf 113(1012–1020):1012–1020
17. Hayat T, Qayyum S, Waqas M, Alsaedi A (2018) Unsteady stagnation point flow of Oldroyd-B nanofluid with heat generation/absorption and nonlinear thermal radiation. J Braz Soc Mech Sci Eng 40:84
18. Ramzan M, Bilal M, Chung JD (2016) MHD stagnation point Cattaneo-Christov heat flux in Williamson fluid flow with homogeneous heterogeneous reactions and convective boundary condition-A numerical approach. J Mol Liq 225:856–862
19. Hayat T, Hussain Z, Farooq M, Alsaedi A (2016) Homogeneous and heterogeneous reactions effects in flow with Joule heating and viscous dissipation. J Mech 33(1):77–86
20. Yasmeen T, Hayat T, Khan MI, Imtiaz M, Alsaedi A (2016) Ferrofluid flow by a stretched surface in the presence of magnetic dipole and homogeneous-heterogeneous reactions. J Mol Liq 223:1000–1005
21. Imtiaz M, Hayat T, Alsaedi A (2016) MHD convective flow of Jeffrey fluid due to a curved stretching surface with homogeneous-heterogeneous reactions. PLoS ONE 11(9):e0161641
22. Hassan M, Zeeshan A, Majeed A, Ellahi R (2017) Particle shape effects on ferrofuids flow and heat transfer under influence of low oscillating magnetic field. J Magn Magn Mat 443:36–44
23. Ellahi R, Tariq MH, Hassan M, Vafai K (2017) On boundary layer nano-ferroliquid flow under the influence of low oscillating stretchable rotating disk. J Mol Liq 229:339–345
24. Majeed A, Zeeshan A, Ellahi R (2016) Unsteady ferromagnetic liquid flow and heat transfer analysis over a stretching sheet with the effect of dipole and prescribed heat flux. J Mol Liq 223:528–533
25. Hayat T, Sajjad R, Ellahi R, Alsaedi A, Muhammad T (2017) Homogeneous-heterogeneous reactions in MHD flow of micropolar fluid by a curved stretching surface. J Mol Liq 240:209–220
26. Lu DC, Ramzan M, Ahmed S, Chung JD, Farooq U (2017) Upshot of binary chemical reaction and activation energy on carbon nanotubes with Cattaneo-Christov heat flux and buoyancy effects. Phys Fluids 29(12):123103
27. Ramzan M, Bilal M, Kanwal S, Chung JD (2017) "Effects of variable thermal conductivity and non-linear thermal radiation past an Eyring Powell nanofluid flow with chemical reaction. Commun Theor Phys 67(6):723
28. Ramzan M, Bilal M, Chung JD (2017) Influence of homogeneous-heterogeneous reactions on MHD 3D Maxwell fluid flow with Cattaneo-Christov heat flux and convective boundary condition. J Mol Liq 230:415–422
29. Ramzan M, Bilal M, Chung JD (2017) Radiative flow of Powell-Eyring magneto-nanofluid over a stretching cylinder with chemical reaction and double stratification near a stagnation point. PLoS ONE 12(10):e0170790
30. Ramzan M, Bilal M, Chung JD, Mann AB (2017) On MHD radiative Jeffery nanofluid flow with convective heat and mass boundary conditions. Neural Comput Appl 1–10
31. Awais M, Hayat T, Muqaddass N, Ali A, Awan SE (2018) Nanoparticles and nonlinear thermal radiation properties in the rheology of polymeric material. Results Phys 8:1038–1045
32. Harris J (1977) Rheology and non-Newtonian flow. Longman, London
33. Schichting H (1964) Boundary layer theory, 6th edn. McGraw-Hill, New York
34. Hayat T, Shehzad SA, Alsaedi A, Alhothuali MS (2013) Three-dimensional flow of Oldroyd-B fluid over surface with convective boundary conditions. Appl Math Mech 34(4):489–500
35. Zargartalebi H, Ghalambaz M, Noghrehabadi A, Chamkha A (2015) Stagnation-point heat transfer of nanofluids toward stretching sheets with variable thermo-physical properties. Adv Powder Technol 26(3):819–829
36. Reddy MG (2013) Chemically reactive species and radiation effects on MHD convective flow past a moving vertical cylinder. Ain Shams Eng J 4:879–888
37. Reddy MG, Sandeep N (2017) Free convective heat and mass transfer of magnetic bio-convective flow caused by a rotating cone and plate in the presence of nonlinear thermal radiation and cross diffusion. J Comput Appl Res Mech Eng 7(1):1–21
38. Bhatti MM, Mishra SR, Abbas T, Rashidi MM (2016) A mathematical model of MHD nanofluid flow having gyrotactic microorganisms with thermal radiation and chemical reaction effects. Neural Comput Appl. https://doi.org/10.1007/s00521-016-2768-8
39. Reddy MG, Sandeep N (2017) Computational modelling and analysis of heat and mass transfer in MHD flow past the upper part of a paraboloid of revolution. Eur Phys J Plus 132:222
40. Bhatti MM, Ali Abbas M, Rashidi MM (2018) A robust numerical method for solving stagnation point flow over a permeable shrinking sheet under the influence of MHD. Appl Math Comput 316(1):381–389
41. Liao SJ (1992) Beyond perturbation. Chapman & Hall/CRC Press, Boca Raton
42. Turkyilmazoglu M (2016) Determination of the correct range of physical parameters in the approximate analytical solutions of nonlinear equations using the adomian decomposition method. Mediterr J Math 13:40194037